Pervaporation of Emulsion Droplets for the Templated Assembly of Spherical Particles: A Population Balance Model

Emily P. Chang, Richard D. Braatz, and T. Alan Hatton
Dept. of Chemical Engineering, Massachusetts Institute of Technology, Cambridge, MA 02139

DOI 10.1002/aic.14146
Published online July 26, 2013 in Wiley Online Library (wileyonlinelibrary.com)

The emulsion droplet solvent evaporation method is used in the preparation of spherical particles, which form due to processes such as the clustering of nanocrystals or precipitation of polymers as the volume of solvent in the droplets decreases. A population balance model is presented to describe this transport of solvent from nanocrystal- or polymer-laden droplets in an emulsion that flows through a pervaporation unit. The solvent transport and lateral migration of droplets was simulated using a high-resolution finite-volume algorithm, which provided a smooth solution with second-order accuracy. Concentration gradients in the continuous phase become prominent when the resistance to solvent transport in the continuous phase dominates that in the membrane. In contrast, with the membrane resistance controlling the overall transport rate, a lumped capacitance assumption can be made and a simpler plug flow model would be sufficient. The simulations also indicate that the particle-size distributions are generally bimodal, and are broader for low dispersed-phase volume fractions and very low-solvent solubilities. Furthermore, the distributions show that radial diffusion of the particles occurs to a significant degree. Such simulations offer insight into how the solvent is removed from emulsion droplets as they flow down a pervaporation fiber and should be useful in the design of pervaporation systems for that purpose. © 2013 American Institute of Chemical Engineers *AIChE J*, 59: 3975–3985, 2013
Keywords: emulsion, evaporation, population balance, pervaporation, mathematical modeling, transport

Introduction

The emulsion droplet solvent evaporation method is widely used in the preparation of nano- and microparticles. Typically, an organic solution of a nonvolatile species is emulsified in an aqueous phase, following which the organic solvent is evaporated, leading to the precipitation of the compound to form particles. One advantage of this method is the ease and efficiency with which numerous lipophilic compounds can be encapsulated, making it appealing for the production of nanoparticles for targeted drug delivery and other medical applications.[1] Uniform poly(lactic acid) and ethylcellulose particles have been prepared using this method,[1–3] while asymmetric Janus beads have been formed upon solvent removal from binary polymer solutions in which the two polymers are both soluble in the solvent at low concentrations, but are immiscible with each other as the solvent volume decreases.[4–9] Water-in-oil emulsions, where the water is evaporated, have similarly been employed for the production of crystalline particles for pharmaceuticals[10,11] and of colloidal clusters of polystyrene or silica microparticles.[12]

Emulsion-based approaches have also been used for the synthesis of colloidal aggregates of particles using nanocrystals comprised of a variety of materials, including semiconducting metal chalcogenides (e.g., sulfides and selenides), metal oxides and rare-earth compounds, as building blocks.[13] In this method, an emulsion (typically an oil-in-water (O/W) system) with the nanocrystals confined to be within the dispersed-phase droplets undergoes controlled evaporation of the solvent, during which the nanocrystals self-assemble into "superparticles." A schematic of the solvent evaporation method is shown in Figure 1.

For O/W emulsions, the low-boiling solvent in the oil phase is simple to remove, and the multitude of nanocrystal building blocks that can be stabilized by surfactant ligands and well-dispersed in nonpolar oils makes this method extremely versatile. Combinations of polymer solutions and nanocrystals in the oil phase are also possible, with polystyrene and poly(lactic acid) nanospheres loaded with iron oxide nanocrystals as two examples.[14,15] Isojima et al. used an oil phase composed of polystyrene and magnetite nanocrystals in a mixture of chloroform and hexane to form Janus particles upon the differential evaporation of the two solvents.[14]

In the aforementioned examples, the conditions under which the solvent was evaporated were central in determining the size and morphology of the polymer nanoparticles or self-assembled "superparticles." Results by Desgouilles et al. suggest that, for sufficiently long evaporation times, emulsion droplets can aggregate and coalesce to eventually form larger polymer nanoparticles, as in the case of ethylcellulose in ethylacetate.[1] Isojima et al. showed that a variety of "superparticle" morphologies could be obtained by varying the processing temperature, and, thus, the solvent evaporation rate.[14] For example, single-domain crystalline

Correspondence concerning this article should be addressed to T. Alan Hatton at tahatton@mit.edu.

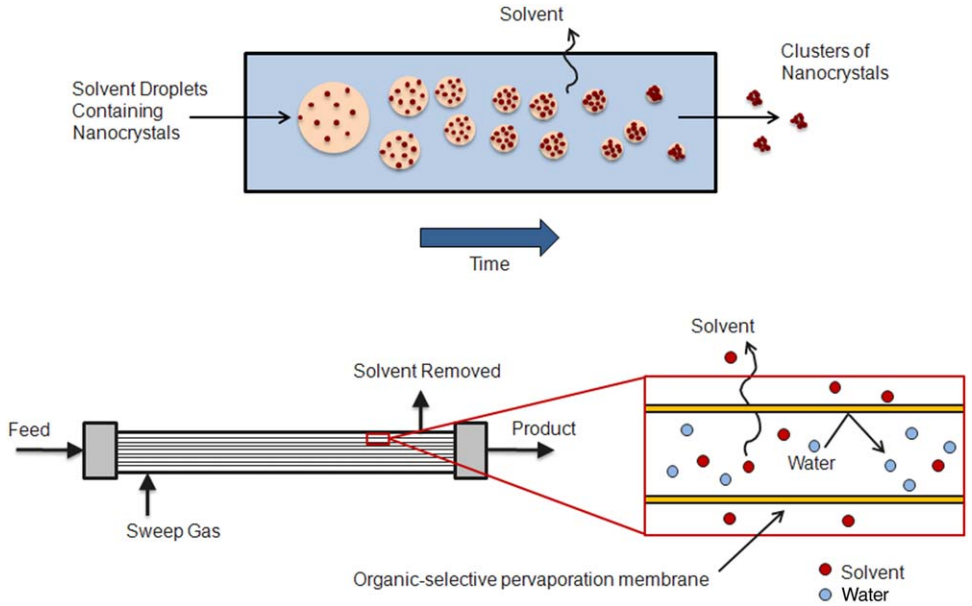

Figure 1. Schematic of the formation of clusters of nanocrystals using the emulsion droplet solvent evaporation method (top), and removal of solvent through an organic-selective pervaporation unit (bottom).

[Color figure can be viewed in the online issue, which is available at wileyonlinelibrary.com.]

superlattices were formed with solvent evaporation at room temperature, whereas toroidal structures formed with temperatures above the solvent boiling point.[14] Furthermore, they showed that, in the case of polystyrene and magnetite nanocrystals dispersed in a mixture of chloroform and hexane, the chloroform must be removed first to form a Janus particle. Hexane is a poor solvent for polystyrene; hence, upon evaporation of the chloroform, the polystyrene precipitated as a bead and the nanocrystal-containing hexane phase accumulated on one side of this bead to accommodate surface energy minimization restrictions. A polystyrene particle partially coated with magnetite nanocrystals remained after the hexane was removed.

These observations indicate that there is a particular need in this method for the control of solvent evaporation rates and the order in which the solvents of a multicomponent system are removed. Moreover, as the desire to produce such complex particles grows commercially, a scalable method for their production is also required. We have recently proposed the use of pervaporation as a means of controlled solvent evaporation for the production of nanoparticles via emulsion-based approaches.[16] Pervaporation is a membrane separation process in which a liquid feed is contacted with one side of the membrane and the permeated product is removed selectively as a vapor from the other side to be condensed or released as desired (see Figure 1). It is commonly used to dehydrate organic solvents, to remove organic compounds from aqueous solutions and to separate anhydrous organic mixtures.[17] The rate at which a compound is transported through the membrane is controlled by the permeability of that compound within the membrane; the driving force for the mass transport is the chemical potential gradient across the membrane, which can be created by either applying a vacuum or flowing an inert purge gas on the permeate side. Typical membranes are composed of silicone rubber, cellulose acetate, nitrile-butadiene, and styrene-butadiene copolymers.[18]

The solvent transport from the droplets through the continuous phase and out of the membrane is complex because, even if the entering droplets are monodisperse, diffusive and convective forces drive the droplets down different paths through the unit, causing them to lose solvent at different rates. The behavior of the droplets can be described by a population balance model, which is a balance on a defined set of dispersed entities, such as particles of a given size, that accounts for the net accumulation of these entities in a given system as a result of all phenomena that add and remove the entities from the set. Population balances are used in many chemical processes involving particulate systems, such as polymerization, solution crystallization, cloud formation and cell dynamics.[19] Population balances are characterized by both internal and external coordinates, where the internal coordinates represent quantities associated with the particle (e.g., size, composition, temperature), and the external coordinates denote the spatial position of the particle. The general population balance equation for the number density n of entities of a particular size includes accumulation, convective, diffusive, and growth terms, as well as terms representing birth and death processes due to aggregation and breakage of particles. The equation is often of the integropartial differential form, and several solution methods have been developed over the past two decades, including discretization and finite-element methods, and the method of moments.[19,20]

This article presents a high-resolution finite-volume algorithm to solve a population balance model for the removal of solvent from dispersed-phase emulsion droplets flowing through a hollow fiber pervaporation unit. The model system is an emulsion composed of a solvent containing suspended nanocrystals or dissolved polymers dispersed stably as droplets within a continuous phase flowing through one of the many cylindrical fibers in the pervaporation unit. Typical emulsions of interest include hexane, toluene, chloroform, or ethyl acetate dispersed in an aqueous continuous phase, or water dispersed in a suitable nonvolatile organic phase, such as dodecane. For simplicity of nomenclature, we will refer to the dispersed phase as the solvent, although the system may be either oil in an aqueous phase or water in an organic

phase. Such a model enables the evaluation of overall mass-transfer rates in the removal of solvent from the unit, and provides insight into the evolution of the droplet populations with time, and into relative solvent transport rates within the flowing fluid and across the membranes.

Model Development

In our process, all droplets shrink (but do not break) to particles of finite final size as determined by the volume of the nanocrystals or polymers inside each droplet. Additionally, the emulsion droplets are assumed to have sufficient steric or charge stabilization that they remain separate and distinct, i.e., there are no birth or death processes due to aggregation or coalescence of the droplets. Moreover, we ignore possible Ostwald ripening effects and any interparticle interactions that may influence particle diffusion rates. We make the following additional assumptions in deriving the model equations.

The system operates continuously and has reached steady state. It is axisymmetric (no angular variations), and the flow is unidirectional in the axial direction. The Reynolds number is $\mathrm{Re}_d = \rho U d/\mu \sim 0.1$, where ρ and μ are the density and viscosity of the continuous phase, respectively, U is the average velocity, and d is the diameter of the fiber. The hydrodynamic entrance length for a fiber diameter of $d \sim 0.02$ cm is $\sim 10^{-4}$ cm, and so fully developed laminar flow conditions can be assumed.

Under typical operating conditions, the Peclet number for the solvent dissolved in the continuous phase is $Pe_L = LU/D_A \sim 10^4$–10^5, where L is the length of the fiber, and D_A is the solvent molecular diffusion coefficient, while for the dispersed-phase droplets, Pe $\sim 10^7 - 10^8$; thus, axial diffusion of the solvent molecules and droplets relative to the bulk flow can be assumed to be negligible. Moreover, the droplets can be assumed to move at the same velocity as the continuous phase, and, thus, local solvent transport rates between the two phases are effectively those that would occur in a static medium. This is a valid assumption for dilute concentrations with no inertial effects.

Finally, the continuous phase is considered to be saturated with solvent at the entrance to the pervaporation unit, and the concentration of solvent in the purge gas is specified to be negligible (this restriction can be readily relaxed if desired). The membrane is composed of a microporous substrate coated with a thin nonporous solvent-selective layer. The continuous phase wets the pores of the substrate,[21] but its flux through the solvent-selective layer is negligible.

Population balance equation

From the aforementioned assumptions, it follows that the evolution of particles (both solvent droplets that contain nanocrystals/polymers, and polymer nanoparticles or clusters of nanocrystals with all solvent removed) in our pervaporation system can be represented by the following population balance equation (PBE)

$$v_z \frac{\partial n}{\partial z} = D_p \frac{1}{r}\frac{\partial}{\partial r}\left(r\frac{\partial n}{\partial r}\right) - \frac{\partial}{\partial R_p}\left(v_z \frac{dR_p}{dz} n\right) \tag{1}$$

where r and z are the radial and axial coordinates, respectively, v_z is the velocity, D_p is the diffusion coefficient of particles of size (radius) R_p, and $n(R_p, r, z)$ is the number density of particles of size R_p at position (r, z).

The fully-developed laminar conditions imply Hagen-Poiseuille flow, which is characterized by a parabolic velocity profile: $v_z = v_{z,\max}(1 - r^2/R^2)$, where $v_{z,\max}$ is the centerline (maximum) velocity and R is the fiber radius.

The diffusion coefficient of the particles can be calculated from the Stokes–Einstein equation, which is valid for the diffusion of spherical particles through a liquid with a low Reynolds number. Hence, $D_p = k_B T/(6\pi\mu R_p)$, where k_B is the Boltzmann constant, T is the temperature, and μ is the viscosity of the continuous phase.

The emulsification is assumed to produce monodisperse droplets of size R_{p0}. Then the initial overall number density of the droplets is $N_{p0} = \left[V_d/\left(\frac{4}{3}\pi R_{p0}^3\right)\right]/V_{tot} = f_d/\left(\frac{4}{3}\pi R_{p0}^3\right)$, where V_d and V_{tot} are the dispersed-phase and total volumes, respectively, and f_d is the dispersed-phase volume fraction.

Furthermore, because the continuous phase is assumed to be saturated with solvent prior to emulsification, the droplets enter the pervaporation unit with size R_{p0} and only shrink once the solvent begins to be removed from the continuous phase. Therefore, the initial condition is $n(R_p, r, 0) = N_{p0}\delta(R_p - R_{p0})$ and the boundary conditions are $\partial n/\partial r|_{r=0} = 0$ and $\partial n/\partial r|_{r=R} = 0$.

In addition, the derivative $\partial n/\partial R_p$ requires no-flux boundary conditions at the largest and smallest particle sizes to ensure that no particles grow or shrink out of the parameter space.

Growth rate

An expression for dR_p/dz may be derived by performing a mass balance around a single droplet

$$\rho_s \frac{dV_p}{dt} = h_{m,p}\ A_p[C_A(r,z) - C_{Asat}], \tag{2}$$

where ρ_s is the solvent density, V_p and A_p are the droplet volume and surface area, respectively, $h_{m,p}$ is the mass-transfer coefficient for the transport from the droplet to the continuous phase, and C_A and C_{Asat} are the actual and saturated solvent concentrations, respectively, in the continuous phase. The driving force for mass transport is the concentration gradient, which increases as the concentration in the aqueous phase decreases.

Our assumption of a static medium implies an average Sherwood number $\bar{\mathrm{Sh}} = 2$, and, therefore, $h_{m,p} = (D_A/d_p)\bar{\mathrm{Sh}} = D_A/R_p$, where D_A is the diffusion coefficient of the solvent in the continuous phase.

The final kinetic expression is

$$\frac{dR_p}{dz} = \begin{cases} -\dfrac{D_A}{\rho_s v_z}\dfrac{1}{R_p}[C_{Asat} - C_A(r.z)], & R_p > R_{pf} \\ 0, & R_p \le R_{pf} \end{cases} \tag{3}$$

where R_{pf} is the final particle size, as determined by the volume of nanocrystals or dissolved polymers inside the droplets.

Solvent transport equation

An expression is needed for the concentration profile $C_A(r,z)$ in Eq. 3 in order to solve the population balance model. An expression can be determined from a mass balance around a control volume of the continuous phase, leading to

$$v_z \frac{\partial C_A}{\partial z} = D_A \frac{1}{r}\frac{\partial}{\partial r}\left(r\frac{\partial C_A}{\partial r}\right) - \int_0^\infty n(R_p, r, z)\rho_s \frac{dV_p}{dt} dR_p \quad (4)$$

The last term accounts for the solvent entering the continuous phase as it leaves the droplets and depends on the kinetic expression given in Eq. 3.

The initial and boundary conditions are

$$C_A(r, 0) = C_{A0} = C_{Asat} \quad (5)$$

$$\left.\frac{\partial C_A}{\partial r}\right|_{r=0} = 0 \quad (6)$$

$$-D_A \left.\frac{\partial C_A}{\partial r}\right|_{r=R} = k_M[C_A(R) - C_{VA}(R+\delta)] = k_M C_A(R) \quad (7)$$

where C_{VA} is the hypothetical liquid-phase concentration in equilibrium with the gas-phase concentration at the membrane boundary, k_M is the overall mass-transfer coefficient for transport through the composite membrane, R is the inner radius of the membrane and δ is the membrane thickness. Equation 7 assumes that the solvent concentration outside the membrane is negligible.

The overall mass-transfer coefficient of the pervaporation membrane k_M can be determined by adding the resistances to transport in the porous and nonporous layers[21]

$$\frac{1}{k_M} = \frac{1}{k_p(d_{lm}/d_i)} + \frac{1}{S_{M/A}k_{np}(d_o/d_i)} \quad (8)$$

where $S_{M/A}$ is the partition coefficient for the solvent between the nonporous layer and the continuous phase; d_o and d_i are the outer and inner diameters of the fiber, respectively; and the log-mean diameter d_{lm}, and mass-transfer coefficients through the porous (k_p), and nonporous (k_{np}) layers, respectively, are $d_{lm} = (d_o - d_i)/\ln(d_o/d_i)$, $k_p = D_A\varepsilon/(t_p\tau)$, and $k_{np} = D_{np}/t_{np}$, where D_{np} is the diffusion coefficient of the solvent through the nonporous layer; t_p and t_{np} are the thicknesses of the porous and nonporous layers; and ε and τ are the porosity and tortuosity of the porous layer, respectively.[21]

Nondimensionalized problem

Equations 1 and 4 are nondimensionalized with appropriate scaling of the variables

$$r* \equiv \frac{r}{R}, \qquad z* \equiv \frac{z}{v_{z,\max}R^2/D_A}, \qquad C_A* \equiv \frac{C_A}{C_{Asat}},$$
$$R_p* \equiv \frac{R_p}{R_{p0}}, \qquad n* \equiv \frac{R_{p0}n}{N_{p0}}.$$

The radial position, concentration and particle size are scaled with the fiber radius, saturation concentration, and initial droplet size, respectively. The scaling for the axial position is the distance traveled over a time period given by the characteristic time for solvent diffusional transport in the radial direction. The number density per droplet size is scaled by the initial number density divided by the initial droplet size.

The resulting coupled set of partial differential equations, incorporating the kinetic expression from Eq. 3, is

$$(1-r^2)\frac{\partial n}{\partial z} = \begin{cases} \alpha\dfrac{1}{R_p}\dfrac{1}{r}\dfrac{\partial}{\partial r}\left(r\dfrac{\partial n}{\partial r}\right) + \beta(1-C_A)\dfrac{\partial}{\partial R_p}\left(\dfrac{n}{R_p}\right), & R_p > R_{pf} \\ \alpha\dfrac{1}{R_p}\dfrac{1}{r}\dfrac{\partial}{\partial r}\left(r\dfrac{\partial n}{\partial r}\right), & R_p \le R_{pf} \end{cases} \quad (9)$$

$$(1-r^2)\frac{\partial C_A}{\partial z} = \frac{1}{r}\frac{\partial}{\partial r}\left(r\frac{\partial C_A}{\partial r}\right) + \kappa(1-C_A)\int_{R_{pf}}^1 nR_p dR_p \quad (10)$$

All of the variables are in their dimensionless forms, with the * excluded to simplify the notation.

The initial and boundary conditions are

$$n(R_p, r, 0) = \delta(R_p - 1) \quad (11)$$

$$\left.\frac{\partial n}{\partial r}\right|_{r=0} = 0 \quad (12)$$

$$\left.\frac{\partial n}{\partial r}\right|_{r=1} = 0 \quad (13)$$

$$C_A(r, 0) = 1 \quad (14)$$

$$\left.\frac{\partial C_A}{\partial r}\right|_{r=0} = 0 \quad (15)$$

$$\left.\frac{\partial C_A}{\partial r}\right|_{r=1} = -\mathrm{Bi}\, C_A(1) \quad (16)$$

With regard to the $\partial n/\partial R_p$ derivative term in Eq. 9, boundary conditions are placed on n at the largest and smallest R_p to ensure that no particles grow or shrink out of the R_p space, as discussed in the Solution Method section. The dimensionless constants in these equations are

$$\alpha \equiv \frac{D_{p0}}{D_A}, \qquad \beta \equiv \frac{C_{Asat}}{\rho_s}\left(\frac{R}{R_{p0}}\right)^2, \qquad \kappa \equiv 3f_d\left(\frac{R}{R_{p0}}\right)^2,$$
$$\mathrm{Bi} \equiv \frac{k_M R}{D_A}$$

where $D_{p0} = k_B T/(6\pi\mu R_{p0})$ is the initial particle diffusion coefficient and the Biot number Bi is the ratio of the mass-transfer resistance offered by the continuous phase to the membrane mass transfer resistance.

Solution Method

The type of growth problem described earlier is governed by parabolic partial differential equations that were solved numerically. Due to the presence of the internal coordinate (particle size), the PBE is of higher dimensionality than the solvent transport equation. This PBE was first discretized spatially with respect to the internal coordinate R_p to derive a PDE system with only r and z as the dependent variables. Then, a numerical solver was used to solve the coupled equations.

The internal coordinate R_p in the PBE was discretized into N bins, resulting in a system of $N+1$ equations. With this discretization, the solvent transport Eq. 10 becomes

$$(1-r^2)\frac{\partial C_A}{\partial z} = \frac{1}{r}\frac{\partial}{\partial r}\left(r\frac{\partial C_A}{\partial r}\right) + \kappa(1-C_A)\sum_{q=f+1}^{N} n_q R_{p,q}\Delta R_p \quad (17)$$

Discontinuities in the system (e.g., delta function as the initial condition, accumulation of particles of finite final size) result in numerical difficulties if the $\partial n/\partial R_p$ term of the PBE (9) is replaced by classical finite differencing. First-order methods tend to produce numerical diffusion, such that the solution is smeared or damped; most second-order methods produce numerical dispersion, resulting in nonphysical oscillations. In this work, we use a *high-resolution method* that provides second-order accuracy where the solution is smooth and does

Table 1. Summary of Relevant Properties for Representative Solvents of Interest

Dispersed Phase	Continuous Phase	C_{Asat} (g/L)[24–27]	ρ_s (g/mL)[24,25]	P	D_A (cm^2/s)[25, 28–32]
Hexane	Water	0.01	0.66	1.5×10^{-5}	8×10^{-6}
Toluene	Water	0.5	0.86	5.8×10^{-4}	9×10^{-6}
Chloroform	Water	8	1.48	5.4×10^{-3}	1×10^{-5}
Ethyl Acetate	Water	80	0.90	8.9×10^{-2}	1×10^{-5}
Water	Hexadecane	0.04	1.00	4.0×10^{-5}	1×10^{-5}
Water	Dodecane	0.05	1.00	5.0×10^{-5}	2×10^{-5}
Water	Toluene	0.5	1.00	5.0×10^{-4}	6×10^{-5}

not introduce numerical dispersion (for detailed descriptions of such methods see Ref. 22 and 23 and citations therein).

The high-resolution scheme used to approximate the derivative in the PBE is

$$\frac{\partial}{\partial R_p}\left(\frac{n}{R_p}\right)\approx\left(\frac{n_{i+1}/R_{p,i+1}}{\Delta R_p}-\phi_{i+1}\frac{n_{i+1}/R_{p,i+1}-n_i/R_{p,i}}{2\Delta R_p}\right)-\left(\frac{n_i/R_{p,i}}{\Delta R_p}-\phi_i\frac{n_i/R_{p,i}-n_{i-1}/R_{p,i-1}}{2\Delta R_p}\right) \tag{18}$$

The first half of the righthand side represents the inward flux to bin I, and the second half is the outward flux. The flux-limiter function $\phi_i=\phi\ (\theta_i)$ depends on the smoothness of the distribution, which is quantified by the ratio of two consecutive gradients

$$\theta_i=\frac{\left(n_{i+1}/R_{p,i+1}\right)-\left(n_i/R_{p,i}\right)}{\left(n_i/R_{p,i}\right)-\left(n_{i-1}/R_{p,i-1}\right)} \tag{19}$$

The characteristics and options for flux-limiter functions are discussed elsewhere.[22,23] This work uses the Van Leer flux limiter

$$\phi_i=\frac{|\theta_i|+\theta_i}{1+|\theta_i|} \tag{20}$$

It can be shown that, for very large gradients ($\phi_i=2$) or negative and zero gradients ($\phi_i=0$), this algorithm is nearly identical to first-order differencing. For intermediate gradients ($\theta_i\sim1,\ \phi_i=\phi_{i+1}$), the algorithm is nearly identical to second-order (centered) differencing.

The no-flux boundary conditions on R_p imply that particles do not shrink into or out of the system. To implement these conditions, the high-resolution term has no inward flux for the largest particle size, and no outward flux for the smallest particle size. That is, the equations for n_i, where $i=f$ (the smallest particle size) and $i=N$ (the largest particle size), are

$$\left(1-r^2\right)\frac{\partial n_f}{\partial z}=\alpha\frac{1}{R_{p,f}}\frac{1}{r}\frac{\partial}{\partial r}\left(r\frac{\partial n_f}{\partial r}\right)+\beta(1-C_A)\times\left(\frac{n_{f+1}/R_{p,f+1}}{\Delta R_p}-\phi_{f+1}\frac{n_{f+1}/R_{p,f+1}-n_f/R_{p,f}}{2\Delta R_p}\right), \tag{21}$$

$$\left(1-r^2\right)\frac{\partial n_N}{\partial z}=\alpha\frac{1}{R_{p,N}}\frac{1}{r}\frac{\partial}{\partial r}\left(r\frac{\partial n_N}{\partial r}\right)+\beta(1-C_A)\times\left(\phi_N\frac{n_N/R_{p,N}-n_{N-1}/R_{p,N-1}}{2\Delta R_p}-\frac{n_{N-1}/R_{p,N-1}}{\Delta R_p}\right). \tag{22}$$

For all other i, the PBE with discretized internal coordinate R_p is

$$\left(1-r^2\right)\frac{\partial n_i}{\partial z}=\alpha\frac{1}{r}\frac{\partial}{\partial r}\left(\frac{1}{R_{p,i}}r\frac{\partial n_i}{\partial r}\right)+\beta(1-C_A)\left(\frac{n_{i+1}/R_{p,i+1}-n_i/R_{p,i}}{\Delta R_p}+\phi_i\frac{n_i/R_{p,i}-n_{i-1}/R_{p,i-1}}{2\Delta R_p}-\phi_{i+1}\frac{n_{i+1}/R_{p,i+1}-n_i/R_{p,i}}{2\Delta R_p}\right). \tag{23}$$

Equations 17 and 21–23 were solved using the Matlab solver *pdepe* subject to the initial and boundary conditions for C_A given in Eqs. 14–16 and for the n_i given by

$$n_i(r,0)\Delta R_{pi}=\begin{cases}1, & i=N\\ 0, & i\neq N\end{cases} \tag{24}$$

$$\left.\frac{\partial n_i}{\partial r}\right|_{r=0}=0 \tag{25}$$

$$\left.\frac{\partial n_i}{\partial r}\right|_{r=1}=0 \tag{26}$$

Model Parameters

Relevant properties for some representative solvents of interest in the emulsion solvent evaporation method for particle preparation are listed in Table 1.

The partition coefficient P is the ratio C_{Asat}/ρ_s. The value for C_{Asat} was approximated as the solubility of each solvent in the continuous phase at 20°C since the volume fraction of the dispersed phase is generally quite small. These solvents were chosen because their solubilities vary widely across different orders of magnitude. Moreover, they have all been reported in the literature for use in the emulsion droplet solvent evaporation method: hexane-in-water for magnetite clusters or Janus beads containing primary magnetite nanoparticles;[14] toluene-in-water for PS/PMMA Janus beads;[4] chloroform-in-water for PS/PPC and PFB/F8BT Janus beads;[5] ethyl acetate-in-water for ethyl cellulose and poly(-lactic acid) particles;[1] water-in-toluene and water-in-hexadecane for colloidal clusters of polystyrene and silica microparticles, respectively;[12] and water-in-dodecane for crystalline glycine particles.[10,11]

Typical parameter values for the emulsification and pervaporation systems in our laboratory are listed in Table 2.

The mass-transfer coefficient of the solvent through the membrane k_M, depends on the resistances of the porous and nonporous layers, which have thicknesses of 30 μm and 400 nm, respectively, in our system. Typical ranges of the porosity and

Table 2. Operating Parameters as used in Ref. 16

Parameter	Value
Number of fibers	180
Fiber radius	0.12 mm
Fiber length	180 mm
Flow rate through unit	0.1 mL/min
Temperature	298 K
Dispersed-phase volume fraction f_d	0.03
Initial droplet radius R_{p0}	645 nm
Final droplet radius R_{pf}	100 nm

tortuosity for porous supports are 0.4–0.83 and 1–3, respectively.[33] The permeability, which is the product of D_{np} and $S_{M/A}$, of hexane in a polysiloxane membrane is known to be 9.4×10^{-7} cm^3 (STP) · cm/(s · cm^2 · cmHg),[34] which is equivalent to about 7.8×10^{-5} cm^2/s for an ideal gas at 300 K. With these values, k_M for our membrane would be on the order of 10^{-4} cm/s.

Representative ranges of values for the four dimensionless constants, based on the physical properties of the solvents (e.g., as in Table 1) and other realistic process parameters (e.g., as given in Table 2), are shown in Table 3.

Results and Discussion

We have formulated a population balance model to describe the transport of solvent in an emulsion passing through a pervaporation hollow fiber membrane as the solvent is lost first from the emulsion droplets to the continuous phase and is then removed by a sweep stream on the shell side of the membrane. Continuous-phase solvent concentration profiles obtained from these simulations for three different Biot numbers are shown in Figure 2 for the conditions $\alpha = 4 \times 10^{-4}$, $\beta = 0.1$, and $\kappa = 100$, which represent a low dispersed-phase volume fraction of a low-solubility solvent such as hexane in water. For low Biot numbers, e.g., Bi = 0.1, the transport resistance within the continuous phase is much lower than that offered by the membrane; thus, there is little variation in the continuous-phase concentration across the fiber cross section, and it remains close to saturation throughout the fiber interior, as indicated by the red color in the figure. As the solvent in the continuous phase is removed through the membrane, it is replenished from the reservoir of solvent in the droplets; it is only when the particles are dry that the remaining solvent is removed rapidly and the continuous-phase concentration drops sharply to zero. In contrast, concentration gradients become more prominent with higher Bi, when the transport resistance offered by the continuous phase is commensurate with or exceeds that of the membrane, and the solvent is removed more quickly than when the membrane resistance is relatively higher. This pattern, where significant concentration gradients, particularly in the radial direction, are only observed for Bi ≥ 1, was consistent across all simulated conditions (e.g., higher solubility solvents, larger oil-phase volume fraction).

Table 3. Ranges of Dimensionless Constants

Dimensionless Constant	Range
$\alpha = D_{p0}/D_A$	4×10^{-5} – 1×10^{-3}
$\beta = (C_{Asat}/\rho_s)(R/R_{p0})^2$	0.05 – 5×10^4
$\kappa = 3f_d(R/R_{p0})^2$	10 – 8×10^4
Bi $= k_M R/D_A$	0.01 – 10

The impact of the dimensionless constants α, β, κ, and Bi on the rate of solvent removal was assessed through a parametric study, in which we used as a metric the dimensionless fiber length at which essentially all solvent is removed z_f^*, i.e., the position at which the dimensionless concentration in the aqueous phase at the wall ($C_A(R)$) dropped to 10^{-6}. The value of z_f^* will vary depending on the cut-off value for $C_A(R)$ in many cases, but the trend is the same as long as the cut-off value is consistent across all simulations. Note that for this position, we will use z_f and z_f^* to denote the dimensional and dimensionless values, respectively.

The dimensionless constant α represents the ratio of the diffusion rate of the initial droplets to that of the solvent in the continuous phase, and the constant β is proportional to the solvent solubility, which can vary widely (see Table 3). For very low β, z_f^* decreases with increasing α, since, for solvents with low solubilities, the diffusion of droplets through the continuous phase is important and contributes to the overall solvent transport rate. However, over the practical operating parameter ranges, α is small in comparison to β, and on inspection of Eq. 9, it is clear that α would have a negligible effect on the solvent transport rate, except in cases of very low β. Indeed, the simulation results show that even at $\beta = 0.1$, z_f^* varies by less than twofold over a 10^4-fold range of α.

A summary of the results for the effects of variations in β, κ, and Bi on z_f^* is shown in Figure 3. The ordinate variable $\varsigma = 12 z_f^* \mathrm{Bi}\,\beta/\kappa = 2\pi R z_f k_M C_{Asat}/(\langle v_z \rangle \pi R^2 f_d \rho_s)$ represents the membrane fiber length required for complete removal of the solvent z_f, relative to the fiber length $z_{f,\min} = \langle v_z \rangle \pi R^2 f_d \rho_s/(2\pi R k_M C_{Asat})$ that would be required if the rate of solvent removal from the droplets were at its maximum possible value (which would occur *if* the continuous phase were at the saturated concentration C_{Asat},

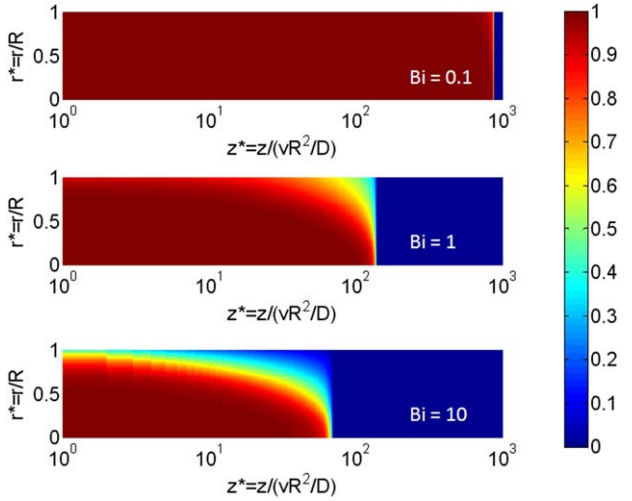

Figure 2. Continuous-phase concentration profiles for $\alpha = 4\times10^{-4}$, $\beta = 0.1$, and $\kappa = 100$ for different Bi.

[Color figure can be viewed in the online issue, which is available at wileyonlinelibrary.com.]

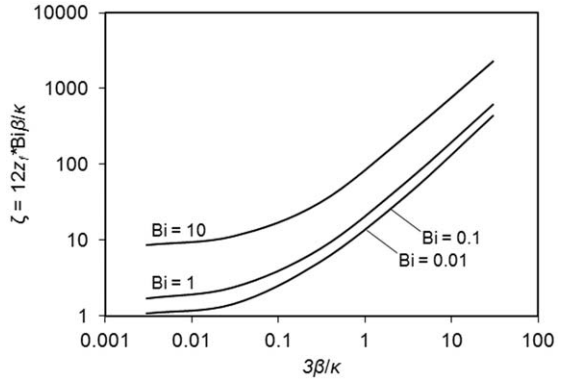

Figure 3. The combined parameter $12z_f^*\mathrm{Bi}\beta/\kappa = 2z_f k_M C_{Asat}/(\langle v_z\rangle R f_d \rho_s)$, which represents an inverse effectiveness factor for solvent transport through the membrane, as a function of $3\beta/\kappa = C_{Asat}/(f_d\rho_s)$ for different Bi.

everywhere).[†] Thus, ζ can be interpreted as an inverse effectiveness factor and must be greater than or equal to unity since transport through the membrane under saturated conditions occurs at the maximum rate and can be significantly greater than the transport when the continuous phase is undersaturated. The abscissa variable $3\beta/\kappa = C_{Asat}/f_d\rho_s$, in Figure 3 represents the solvent capacity in the continuous phase relative to the total solvent in the feed dispersed phase, per unit volume of emulsion (assuming that the initial crystal or polymer volume fraction in the dispersed phase is small).

The relationship between the solvent transport rate and $C_{Asat}/f_d\rho_s$ can be divided into two regimes. For $C_{Asat}/f_d\rho_s > 1$, z_f remains fairly constant (and, thus ζ vs. $C_{Asat}/f_d\rho_s$ is linear) for a given Bi because the continuous phase already has the capacity to dissolve all of the solvent in the droplets, and increasing this capacity would not significantly increase the driving force for transport out of the droplets. In contrast, for $C_{Asat}/f_d\rho_s < 1$, increasing the solvent solubility or lowering the dispersed-phase volume fraction would increase the transport rate. The ratio $C_{Asat}/f_d\rho_s$ (or β/κ) can be adjusted by changing to a solvent with different physical properties or by using a different dispersed-phase volume fraction.

The results for z_f^* are insensitive to Bi for $\mathrm{Bi} \ll 1$, as indicated by the overlapping curves for Biot numbers 0.01 and 0.1 for all values of $C_{Asat}/f_d\rho_s$, since the membrane dominates the overall transport in the system under these conditions. In contrast, Biot numbers greater than one signify that the resistances offered by the fluid phase control the overall transport rates, and the trans-membrane driving force is less than if the concentration were uniform over the flow cross section. For $\mathrm{Bi} >> 1$, further increases in the membrane mass-transfer coefficient have no impact on the overall solvent transport rate, and z_f becomes independent of Bi.

The evolution of the particle-size distribution as the emulsion is convected through the fiber was also studied. The mixing-cup average particle-size distribution $\int_0^1 n(R_p,r,z)v_z(r)2\pi r dr \Big/ \int_0^1 v_z(r)2\pi r dr$ at various axial positions is shown in Figure 4 for different solvent solubilities ($\beta = 0.1$ and 10) and dispersed-phase volume fractions ($\kappa = 100$ and 1000); this average is representative of the size distribution of particles discharged from a fiber of the given length accounting for radially-dependent particle velocities and is different from the simple radially-averaged size distribution. The particles are monodisperse at $z = 0$, but bifurcate into two different populations, one population representing particles from which all solvent has been removed, and which grows with increasing z (the left peak), and the other population giving the size distribution of droplets that still contain solvent and are in the process of shrinking (the right peak); this latter peak becomes smaller with increasing z.

For $\beta = 10$ and $\kappa = 100$, most (~80%) of the particles are dry within the first 20% of the length taken for complete removal of the solvent from the emulsion, and the remaining 80% of z_f is required for removal of the residual dissolved solvent from the continuous phase through the membrane. The same drying pattern is achieved with $\kappa = 1000$ provided that $\beta \sim 1000$. In contrast, for $\beta = 10$ and $\kappa = 1000$, more than 60% of z_f is required for about 80% of the particles to be dried and less than 40% of z_f is used for residual solvent removal. For $\kappa = 1000$ and $\beta = 0.1$, over 90% of z_f is required to dry just over half the particles. These results regarding the rate at which the particles become dry relative to the rate at which the solvent is completely removed from the emulsion show that, with higher solubility solvents, a larger proportion of the overall solvent transport time is devoted to removing the residual solvent from the continuous phase after the particles are dry because, as the pervaporation began under saturated initial conditions, more solvent would have been dissolved in the

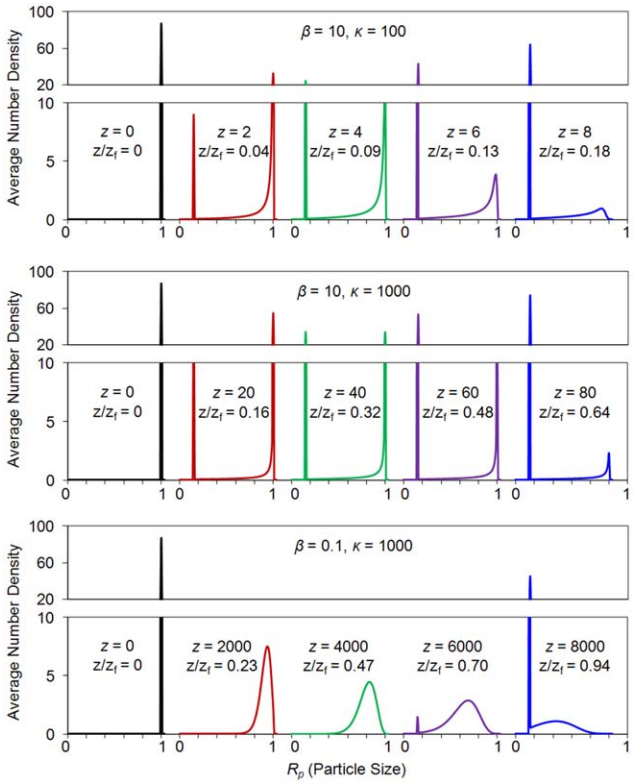

Figure 4. Mixing-cup average particle size distributions at different axial positions for different β and κ conditions.

The other dimensionless constants were $\alpha = 4 \times 10^{-4}$ and $\mathrm{Bi} = 0.1$. [Color figure can be viewed in the online issue, which is available at wileyonlinelibrary.com.]

[†]*Strictly speaking, the numerator of $z_{f,\min}$ should be $\langle v_z\rangle\pi R^2[f_d(1-\phi)\rho_s]$, where $\phi = (R_{pf}/R_{p0})^3$ is the volume fraction of crystals or polymers in the dispersed phase feed to the membrane unit. For small ϕ, this quantity can be approximated by $\langle v_z\rangle\pi R^2 f_d\rho_s$.*

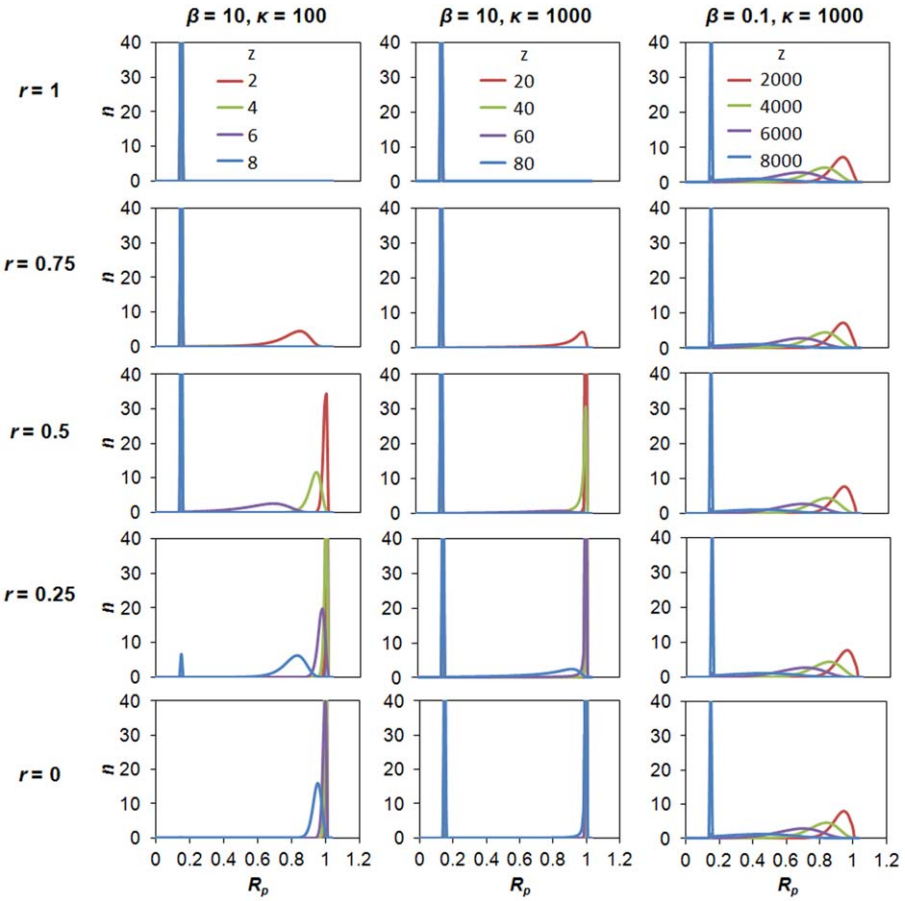

Figure 5. Particle-size distributions at different radial positions for different β and κ conditions.

The other dimensionless constants were $\alpha = 4 \times 10^{-4}$ and Bi = 0.1. For each radial position, the distribution at each axial position is shown. [Color figure can be viewed in the online issue, which is available at wileyonlinelibrary.com.]

continuous phase to begin with. Moreover, with very low dispersed-phase volume fractions (low κ), or very soluble solvents (high β), the continuous phase has sufficient capacity to extract most of the solvent from the droplets very early into the process; thus, there is very little solvent in the dispersed phase remaining to replenish the solvent in the continuous phase as it is removed by diffusional processes through the continuous phase to the membrane and subsequently across the membrane itself.

The evolution of the particle-size distribution with increasing residence time in the pervaporation fiber is likewise noticeably different for different β and κ conditions. In terms of the mean and variance that characterize the distributions, a low κ with a high β, or a very low β with a high κ, both result (although for different reasons to be discussed below) in the peak at the right shifting to the left and broadening before the solvent is completely removed from all of the particles. This effect is more evident for the latter case. Conversely, if both β and κ are higher, the majority of the particles at all axial positions appear to be either of size R_{pf} or of size R_{p0}, with few particles of intermediate size.

Additional insight into these distributions can be gained by inspection of the particle size distributions at different radial positions as they evolve with residence time in the fibers (see Figure 5). For both $\kappa = 100$ and $\kappa = 1000$ at $\beta = 10$, only dry particles of size R_{pf} are observed at the wall ($r = 1$) with no larger solvent-containing particles. This indicates that, in these cases, any solvent in the droplets is immediately removed once they reach the wall. However, consistent with the particle-size distributions in Figure 4, the particle-size distributions show more variation with radial position within the fiber with $\kappa = 100$ than with $\kappa = 1000$ at $\beta = 10$. For $\kappa = 100$, the particle-size distribution shifts rapidly toward the left with increasing z, particularly in regions closer to the wall. For example, for $r = 0.75$ at a travel distance of only $z = 2$, about 20% of the particles are already dry and the average droplet size of the remaining droplets is about 85% of the initial droplet size. On the other hand, for $\kappa = 1000$, most of the particles between the wall and the center of the fiber are either of size R_{pf} or R_{p0}. This result suggests that, with the larger dispersed-phase volume fraction, there is a sufficiently high concentration of droplets that droplets in the interior of the fiber lose solvent fairly slowly. For a large portion of the droplets, it is only when they reach the wall that they shrink rapidly to R_{pf}, and the appearance of these dry droplets away from the wall is due to their subsequent diffusion back toward the fiber center. The diffusion rates of the dry particles would be significantly greater than those of the solvent-laden particles because of large-size differences, and, thus, the dry particles move away from the wall much more rapidly than the solvent-containing particles move to the wall. This behavior results in a population at each axial position composed primarily of very large droplets and dry (no solvent) particles, but relatively few droplets of intermediate size.

The particle-size distributions at different radial positions for $\beta = 0.1$ and $\kappa = 1000$ were, interestingly, all roughly the same as the overall distribution shown in Figure 4. The

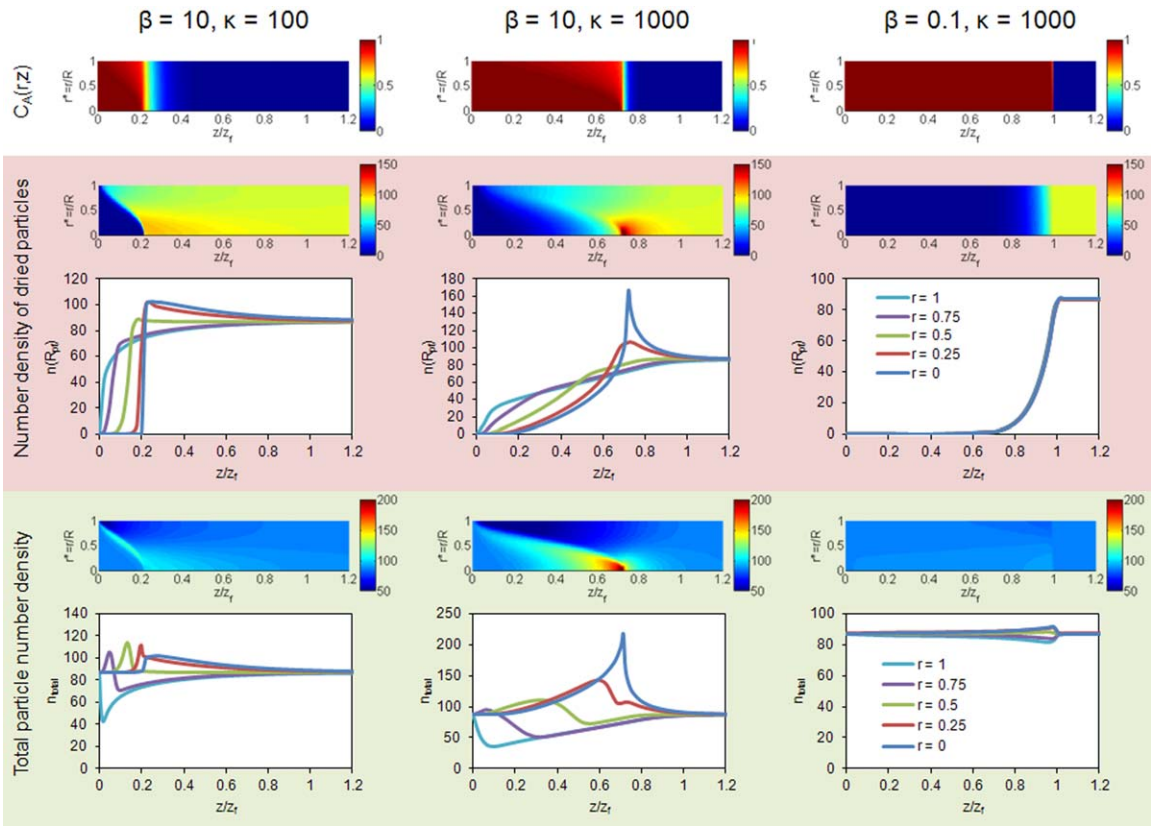

Figure 6. The concentration profile (top), number density of particles of size R_{pf} (middle), and the total number density of all particles (bottom) as a function of radial and axial position for different β and κ conditions.

radial particle diffusion rate is significant compared to the solvent transport rate because of the very low solubility of the solvent in the continuous phase, resulting in essentially the same particle-size distributions across the radial direction that all gradually shift to the left with increasing z. The solvent is removed very slowly due to the large amount and low solubility of the solvent that prevents a significant amount of the solvent from leaving the droplets for the continuous phase at any given time. In contrast to the conditions with $\kappa = 100$ and 1000 at $\beta = 10$, the droplets do not immediately dry out upon reaching the wall because the solvent solubility limitations are quite severe.

Particle density profiles are shown in Figure 6, where the plots in the middle and bottom rows display the number densities of particles of size R_{pf} ($n(R_{pf})$) and of all particles (n_{total}), respectively, as functions of the spatial coordinates. The corresponding solvent concentration profiles are displayed at the top of the figure. The dimensionless quantity $\tau = \left(z_f/\langle v_z \rangle\right)/\left(R^2/D_p\right)$, compares the timescale for solvent removal (i.e., the time required to travel a distance z_f down the fiber) with the timescale for radial particle diffusion (R^2/D_p). In general, by analogy with diffusional processes in an infinite cylinder,[35,36] for $\tau > 0.2$, particles at the fiber walls can be assumed to have penetrated, by diffusion, significantly into the fiber center. The diffusion of dry particles, with $\tau \sim 0.65$, toward the fiber center is evident, as the maximum of $n(R_{pf})$ occurs at the fiber center at the axial position at which all particles become dry. After all of the particles are dry, the particles continue to diffuse radially until the number density is uniform across the entire fiber.

For the $\beta = 0.1$ case, consistent with previous observations, there is uniformity across the fiber cross section for the entire length of the fiber in terms of the particle size distribution. For the $\beta = 10$ cases, interesting wavy behavior in

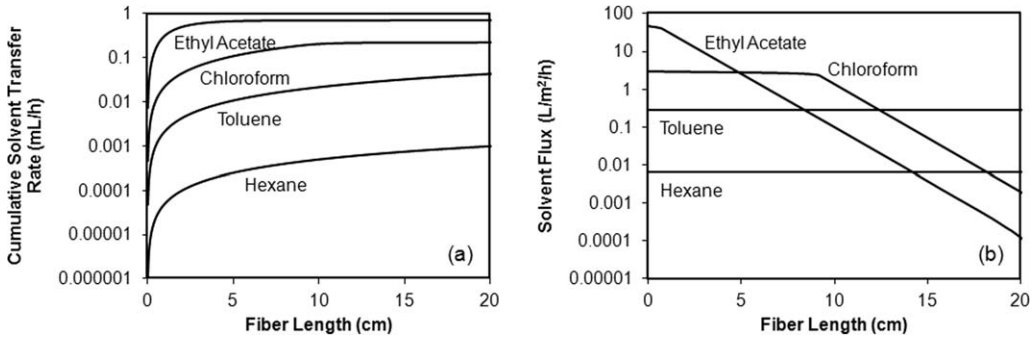

Figure 7. (a) Cumulative solvent transfer rate, and (b) flux as a function of axial position for different organic solvents.

These rates were computed for a Bi of 0.1, total emulsion flow rate of 0.1 mL/min through a 180-fiber pervaporation unit, and oil-phase volume fraction of 0.03.

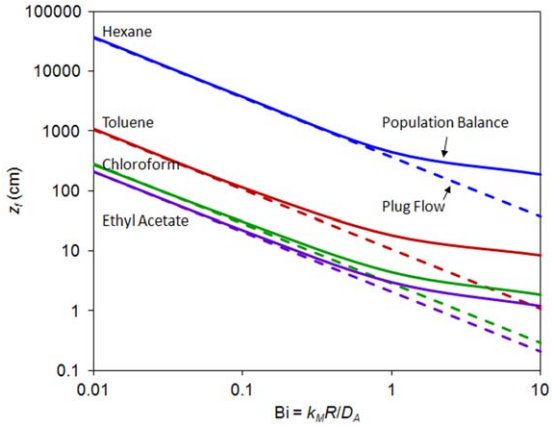

Figure 8. The fiber length at which all solvent is removed in cm, as predicted by the population balance and plug flow models for different solvents under Biot numbers ranging from 0.01 to 10.

[Color figure can be viewed in the online issue, which is available at wileyonlinelibrary.com.]

the total particle density at different radial positions results from the diffusion of the dry particles toward the center, which is faster than diffusion of wet particles toward the wall, momentarily increasing the total number density of the particles at each radial position; when the wet particles at those positions dry out, these peaks dissipate as the dry particles diffuse away owing to the concentration gradient driving force established in that region on drying of the wet particles. The spatial variations are sharper near the entrance for the low dispersed-phase volume fraction $\kappa = 100$, where the changes in particle density occur relatively quickly due to the small amount of solvent that must be removed. In the case of $\kappa = 1000$, the simulations show that, while C_A across the fiber is high, the particles only become dry at the wall, after which they diffuse away from the wall to the fiber center, to distribute quite evenly over the tube cross section, so that the average number density of the dry droplets even at the center of the tube approaches the feed density n_0; similarly, the large droplets of initial size R_{p0}, for which $\tau \sim 0.1$, initially at the fiber center do not migrate significantly from the center of the tube, so their number density remains close to the feed density, i.e., to n_0. Thus, the *total* number density of particles at the center of the tube approaches the sum of these two particle densities, i.e., $n_{total} \sim 2n_0$. Once C_A falls significantly, however, the driving force for solvent transport through the continuous phase to the membrane surface is sufficiently large to allow for complete drying of the wet particles originally confined to the fiber center; the large spike in the number density at $r = 0$ near $z/z_f = 0.7$ is therefore due to both dry particles that have diffused to the center from the wall and particles that had been in the fiber center from the beginning, and only lost all of their solvent at the very end, so the concentration of dry particles approaches a number density of $2n_0$. This sudden increase in concentration of the smaller particles at the center generates a large driving force for diffusion of these particles away from the center to redistribute over the entire flow cross section, and, hence, the rapid decay in the number density of particles at the center of the flow; the time constant for this decay in center line number density is consistent with the characteristic radial diffusional time for entities of the size of the dry particles.

Simulation results for aqueous dispersions of the four representative organic solvents listed in Table 1, which have a wide range of solvent transport rates and fluxes due to their different physical properties, are presented in Figures 7 and 8. Solvent transport rates are higher for more soluble solvents, i.e., larger β, which determines the magnitude of the term in the population balance equations that governs the rate of the change in the particle-size distribution due to the shrinking of the droplets. This coefficient varies by orders of magnitude between the different solvents due to their solubility differences.

Solvent transfer rates and fluxes through the membrane as functions of axial position are shown in Figure 7 for a Biot number of 0.1 and other conditions listed in Table 2. The cumulative solvent transfer rate is the total volume of solvent removed per hour for a given length of fiber, and therefore provides an indication as to what flow rates are reasonable to use for a certain unit size. The maximum cumulative solvent transfer rate must equal the flow rate of solvent into the unit, and achieving that rate at a particular axial position would imply that all solvent is removed by that point within the unit. It is evident that complete solvent removal within one pass through an 18 cm bench scale unit is realistic when the more water-soluble organic solvents are used. For the less soluble solvents toluene and hexane, the solvent flux remains constant and low, such that much longer residence times would be required to remove all of the solvent.

In earlier work, we had developed a simpler model to describe the solvent transport from emulsions flowing through pervaporation fibers.[16] The model assumed plug flow with no solvent concentration or droplet-size variations in the radial direction. This assumption is valid if the solvent diffusion rate through the aqueous phase is so fast relative to transport through the membrane that there is essentially complete mixing and, hence, uniformity, across the fiber. Our simulation results confirm that such uniformity is achieved under lumped capacitance conditions, where the Biot number is ~0.1 or lower (Figure 2).

Indeed, as shown in Figure 8, the plug flow and population balance models predict similar values for the fiber length at which all solvent is removed (given the parameters listed in Table 2) for $\mathrm{Bi} \leq 0.1$, where the relationship between z_f and Bi is linear. The percent error in the values of z_f estimated using the plug flow model as compared to those calculated using the population balance model relative to the PB predictions, generally decreases with decreasing Bi; the percent error is less than 10% for all of the simulations where $\mathrm{Bi} \leq 0.1$, but ~30–40% for $\mathrm{Bi} = 1$, and greater than 80% for $\mathrm{Bi} = 10$.

Conclusions

A population balance model has been developed to describe the transport of solvent from nanoparticle- or polymer-laden emulsion droplets flowing through pervaporation fibers. The solvent diffuses from the droplets into the surrounding aqueous medium and leaves the system via diffusion through the pervaporation membrane. We have proposed pervaporation as an effective and well-controlled solvent removal method for the clustering of primary nanoparticles or the precipitation of polymers to form spherical particles.[16]

The model is comprised of a coupled set of partial differential equations describing the steady-state solvent concentration in the aqueous phase and the number of particles of a

particular size as functions of the radial and axial positions in a fiber. The model equations were solved using a high-resolution finite volume algorithm, where a flux-limiter function was used to provide a numerically reliable solution with second-order accuracy.

The simulation results provide information regarding the effect of various parameters on the solvent transport, and the behavior of the droplets while flowing through the pervaporation fibers. Furthermore, the required fiber length to remove the solvent completely from an emulsion can be determined in terms of natural dimensionless constants that arise from the structure of the model equations, as shown in Figures 3 and 8. Such plots may be used as design tools for pervaporation units to be used in the solvent removal from emulsions. The model is applicable to both O/W and W/O emulsions and it is straightforward to modify the equations to fit solvent evaporation configurations other than a hollow pervaporation fiber. For example, the population balance model and algorithm developed here may be used to analyze the solvent evaporation from an emulsion sitting on a heated flat substrate, such as that described by Toldy et al.[11] or a similar substrate that is inclined to provide for a flow system. In future studies, we may also relax some of the assumptions to solve more complex problems, for instance, multi-solvent systems where the concentration of both solvents in the sweep gas must be controlled, or systems in which particle–particle interactions and particle aggregation are important.

Acknowledgment

Financial support from the Singapore-MIT Alliance is gratefully acknowledged.

Literature Cited

1. Desgouilles S, Vauthier C, Bazile D, Vacus J, Grossiord J, Veillard M, Couvreur P. The design of nanoparticles obtained by solvent Evaporation. *Langmuir*. 2003;19:9504–9510.
2. Katou H, Wandrey AJ, Gander B. Kinetics of solvent extraction/evaporation process for PLGA microparticle fabrication. *Int J Pharma*. 2008;364:45–53.
3. Sawalha H, Purwanti N, Rinzema A, Schroen K, Boom R. Polylactide microspheres prepared by premix membrane emulsification - Effects of solvent removal rate. *J Membr Sci*. 2008;310:484–493.
4. Saito N, Kagari Y, Okubo M. Effect of colloidal stabilizer on the shape of polystyrene/poly(methyl methacrylate) composite particles prepared in aqueous medium by the solvent evaporation method. *Langmuir*. 2006;22:9397–9402.
5. Kietzke T, Neher D, Kumke M, Ghazy O, Ziener U, Landfester K. Phase separation of binary blends in polymer nanoparticles. *Small*. 2007;3(6):1041–1048.
6. Saito N, Kagari Y, Okubo M. Revisiting the morphology development of solvent-swollen composite polymer particles at thermodynamic equilibrium. *Langmuir*. 2007;23:5914–5919.
7. Saito N, Nakatsuru R, Kagari Y, Okubo M. Formation of "snowmanlike" polystyrene/poly(methyl methacrylate)/toluene droplets dispersed in an aqueous solution of a nonionic surfactant at thermodynamic equilibrium. *Langmuir*. 2007;23:11506–11512.
8. Tanaka T, Nakatsuru R, Kagari Y, Saito N, Okubo M. Effect of molecular weight on the morphology of polystyrene/poly(methyl methacrylate) composite particles prepared by the solvent evaporation method. *Langmuir*. 2008;24:12267–12271.
9. Kietzke T, Neher D, Landfester K, Montenegro R, Güntner R, Scherf U. Novel approaches to polymer blends based on polymer nanoparticles. *Nature Mater*. 2003;2:408–412.
10. Chadwick K, Davey RJ, Mughal R. Crystallization from water-in-oil emulsions as a route to spherical particulates: glycine and the hydrochloride salts of glutamic acid and ephedrine. *Org Process Res Develop*. 2009;13:1284–1290.
11. Toldy AI, Badruddoza AZM, Zheng L, Hatton TA, Gunawan R, Rajagopalan R, Khan SA. Spherical crystallization of glycine from monodisperse microfluidic emulsions. *Crystal Growth Design*. 2012;12:3977–3982.
12. Cho Y, Yi G, Kim S, Pine D, Yang S. Colloidal clusters of microspheres from water-in-oil emulsion. *Chem Mater*. 2005;17:5006–5013.
13. Bai F, Wang D, Huo Z, Chen W, Liu L, Liang X, Chen C, Wang X, Peng Q, Li Y. A Versatile bottom-up assembly approach to colloidal spheres from nanocrystals. *Angew Chem Int Ed*. 2007;46:6650–6653.
14. Isojima T, Suh SK, Vander Sande JB, Hatton TA. Controlled assembly of nanoparticle structures: spherical and toroidal superlattices and nanoparticle-coated polymeric beads. *Langmuir*. 2009;25(14):8292–8298.
15. Urban M, Musyanovych A, Landfester K. Fluorescent superparamagnetic polylactide nanoparticles by combination of miniemulsion and emulsion/solvent evaporation techniques. *Macromol Chem Phys*. 2009;210:961–970.
16. Chang EP, Hatton TA. Membrane emulsification and solvent pervaporation processes for the continuous synthesis of functional magnetic and janus nanobeads. *Langmuir*. 2012;28(25):9748–9758.
17. Feng X, Huang RYM. Liquid separation by membrane pervaporation: A review. *Ind. Eng Chem Res*. 1997;36:1048–1066.
18. Yang D, Majumdar S, Kovenklioglu S, Sirkar KK. Hollow fiber contained liquid membrane pervaporation system for the removal of toxic volatile organics from wastewater. *J Membr Sci*. 1995;103:195–210.
19. Ramkrishna D. Population Balances: Theory and Applications to Particulate Systems in Engineering. San Diego, CA: Academic Press; 2000.
20. Braatz RD. Advanced control of crystallization processes. *Annu Rev Control*. 2002;26:87–99.
21. Abou-Nemeh I, Das A, Saraf A, Sirkar KK. A composite hollow fiber membrane-based pervaporation process for separation of VOCs from aqueous surfactant solutions. *J Membr Sci*. 1999;158:187–209.
22. Gunawan R, Fusman I, Braatz RD. High resolution algorithms for multidimensional population balance equations. *AIChE J*. 2004;50(11):2738–2749.
23. LeVeque RJ. Finite Volume Methods for Hyperbolic Problems. Cambridge, U.K: Cambridge University Press; 2002.
24. Perry RH, Green DW. Perry's Chemical Engineers' Handbook. New York: McGraw-Hill, Inc.; 1999.
25. Regional Screening Level (RSL) Chemical-specific Parameters Supporting Table. 2012. Retrieved from US Environmental Protection Agency. http://www.epa.gov/reg3hwmd/risk/human/rb-concentration_table/Generic_Tables/xls/params_sl_table_run_MAY2012.xls.
26. Maczynski A, Wisniewska-Goclowska, B, Goral M. Recommended liquid-liquid equilibrium data. Part 1. binary alkane-water systems. *J Phys Chem Ref Data*. 2004;33(2):549–577.
27. Neely BJ, Wagner J, Robinson RL, Gasem KAM. Mutual solubility measurements of hydrocarbon-water systems containing benzene, toluene, and 3-methylpentane. *J Chem Eng Data*. 2008;53:165–174.
28. Price WS, Söderman O. Self-diffusion coefficients of some hydrocarbons in water: measurements and scaling relations. *J Phys Chem A*. 2000;104:5892–5894.
29. US Environmental Protection Agency. 1996. Soil Screening Guidance: Technical Background Document. Retrieved from http://www.epa.gov/superfund/health/conmedia/soil/pdfs/part_5.pdf.
30. Lide DR. Diffusion coefficient in liquids at infinite dilution. In: Handbook of Chemistry and Physics. Boca Raton, FL: CRC Press; 2004.
31. Easteal AJ. Tracer diffusion of water in organic liquids. *J Chem Eng Data*. 1996;41:741–744.
32. Su JT, Duncan PB, Momaya A, Jutila A, Needham D. The effect of hydrogen bonding on the diffusion of water in n-alkanes and n-alcohols measured with a novel single microdroplet method. *J Chem Phys*. 2010;132:044506.
33. Krull FF, Fritzmann C, Melin T. Liquid membranes for gas/vapor separations. *J Membr Sci*. 2008;325:509–519.
34. Kuo ACM. Poly(dimethylsiloxane). In: Polymer Data Handbook. Oxford, UK: Oxford University Press, Inc.; 1999.
35. Incropera FP, DeWitt DP. Fundamentals of Heat and Mass Transfer. New York: John Wiley & Sons, Inc.; 2002.
36. Carslaw HS, Jaeger JC. Conduction of Heat in Solids. 2nd ed. London: Oxford at Clarendon Press; 1965.

Manuscript received Mar. 25, 2013, and revision received May 16, 2013.